



Summer temperature changes in Tierra del Fuego since AD 1765: atmospheric drivers and tree-ring reconstruction from the southernmost forests of the world

Vladimir Matskovsky^{1,2} · Fidel A. Roig^{1,3} · Mauricio Fuentes⁴ · Irina Korneva² · Diego Araneo¹ · Hans W. Linderholm⁴ · Juan Carlos Aravena⁵

Received: 7 December 2021 / Accepted: 12 June 2022

© The Author(s), under exclusive licence to Springer-Verlag GmbH Germany, part of Springer Nature 2022

Abstract

Proxy climate records, such as those derived from tree rings, are necessary to extend relatively short instrumental meteorological observations into the past. Tierra del Fuego is the most austral territory with forests in the world, situated close to the Antarctic Peninsula, which makes this region especially interesting for paleoclimatic research. However, high-quality, high-resolution summer temperature reconstruction are lacking in the region. In this study we used 63 tree-ring width chronologies of *Nothofagus pumilio* and *Nothofagus betuloides* and partial least squares regression (PLSR) to produce annually resolved December-to-February temperature reconstruction. The resulting reconstruction extends back to AD 1765 and explains 37–50% of instrumental temperature variability. We found that observed summer temperature variability in Tierra del Fuego is primarily driven by the fluctuations of atmospheric pressure systems both in the South Atlantic and South Pacific, while it is insignificantly correlated to major hemispheric modes: El Niño–Southern Oscillation and Southern Annular Mode. This fact makes our reconstruction important for climate modelling experiments, as it represents specific regional variability. Our reconstruction can be used for direct comparison with model outputs to better understand model limitations or to tune a model. The reconstruction can contribute to larger scale reconstructions based on paleoclimatic data assimilation. Moreover, we showed that PLSR has improved performance over principal component regression (PCR) in the case of multiple tree-ring predictors. According to these results, PLSR may be a preferable method over PCR for the use in automated tree-ring based reconstruction approaches, akin widely used point-by-point regression.

Keywords Southern Hemisphere · *Nothofagus pumilio* · *Nothofagus betuloides* · Dendroclimatology · Southern Atlantic · Partial least squares regression · Principal component regression

1 Introduction

For the last decades, there are indications that many areas of South America have experienced climatic and ecological changes driven by regional, hemispheric-scale, and global ocean–atmosphere processes (Parmesan 2006; Moy et al. 2009). These changes are projected to intensify in the future (Marengo et al. 2009). Long-term, robust climate proxy records provide a baseline against which recent climate variability can be compared, and climate models evaluated to refine their predictive skill. To identify temporal and spatial patterns of climate change, an extensive land proxy network is required. This is problematic for the Southern Hemisphere given low fraction of land and the paucity of sites surveyed at present in various continental sectors. Among different locations in the Southern Hemisphere, the

✉ Vladimir Matskovsky
matskovsky@igras.ru

¹ Institute of Nivology, Glaciology and Environmental Sciences (IANIGLA), CONICET, Mendoza, Argentina

² Institute of Geography, Russian Academy of Sciences, Moscow 119017, Russia

³ Hémera Centro de Observación de La Tierra, Escuela de Ingeniería Forestal, Facultad de Ciencias, Universidad Mayor, Camino La Pirámide 5750, 8580745 Huechuraba, Santiago, Chile

⁴ Regional Climate Group, Department of Earth Sciences, University of Gothenburg, Gothenburg, Sweden

⁵ Gaia Antarctica Research Center, University of Magallanes, 6200000 Punta Arenas, Chile

archipelago of Tierra del Fuego (hereafter TdF), situated at the southern tip of South America, has a privileged position to carry out paleoclimatological studies (Boninsegna et al. 2009; Roig et al. 1996). TdF is the most austral territory with forests in the World, situated close to the Antarctic Peninsula. Besides its unique location, TdF has vast opportunities for paleoclimate studies, as many proxy archives are represented in the region, including peat bogs, lakes, glaciers and trees (Rabassa et al. 1989; Roig et al. 1996). The most detailed (i.e. high resolution) information about the climatic and environmental changes of the last millennia can be obtained from tree-ring records. Robust tree-ring reconstructions of TdF climate can provide information on pre-industrial climate variability in the region, as well as on the atmospheric and oceanic processes behind those. This information is crucial for the advancement of paleoclimatology of the Southern Hemisphere, including paleoclimate modelling. Dendrochronological studies for TdF region were focused on two species: lenga (*Nothofagus pumilio*) and coihue de Magallanes (*N. betuloides*). Another *Nothofagus* species ñire (*N. antarctica*), which is widespread in TdF, have not attracted significant attention of dendrochronologists so far. Research questions of dendrochronological studies in TdF, besides dendroclimatic reconstructions that were described in a review by Boninsegna et al. (2009), included climatic response of tree-ring width chronologies (Massaccesi et al. 2008; Llancabure 2011; Soto-Rogel, Aravena 2017; Matskovsky et al. 2019; Fuentes et al. 2019), potential for development of millennia-long chronologies (Roig et al. 1996), potential application of dendrochronology in silvicultural management (Franco et al. 2019; Mundo et al. 2020), and even a reconstruction of earthquakes of the last 150 years (Pedrera et al. 2014). Still, many questions remain open. One of the important open questions is: are the trees growing in TdF sensitive enough to be used for climate reconstructions?

Another important question that arises when working on a reconstruction is the following: given one climatic parameter reconstructed, what can we say about the regional and/or hemispheric climate variability in the past? Since the climate of TdF is strongly influenced by large-scale atmospheric circulation systems, we may expect a significant connection of regional air temperature with the main Southern Hemispheric atmospheric and ocean-atmospheric modes: the Southern Annular Mode (SAM, also known as the Antarctic Oscillation, AAO) and the El Niño-Southern Oscillation (ENSO). Nevertheless, several studies revealed that linear correlation of summer temperature anomalies with the main atmospheric circulation indices does not confirm this connection. Jacques-Coper and Bronnimann (2014) showed that the correlation coefficients of interannual summer temperature anomalies in Southern South America with ENSO 3.4 and SAM indices for 1907–2001 strongly depend

on the time period. In particular, significant positive correlation was found for several periods in the middle of the twentieth century, but negative correlation with ENSO 3.4 (-0.23) and almost zero with SAM (0.09) was found for the period 1980–2001. According to Marshall et al. (2006), correlation coefficient of summer temperature at Punta Arenas with SAM index was equal to 0.16 . It should be noted that atmospheric circulation indices are simple proxies of large-scale circulation patterns, and they may not be representative for a certain region due to regional variability.

In accordance with the two questions raised, we address two research topics in this study, namely: (i) the suitability of tree-ring data from TdF for summer temperature reconstructions and (ii) the additional information that summer temperature reconstruction from the region may bring to palaeoclimatic research. With this aim in mind, we compiled a set of tree-ring chronologies from TdF, including 44 lenga (*Nothofagus pumilio*) and 19 coihue de Magallanes (*N. betuloides*) chronologies (Boninsegna et al. 1989; Massaccesi et al. 2008; Roig et al. 2010; Llancabure 2011; Soto-Rogel, Aravena 2017; Matskovsky et al. 2019; Fuentes et al. 2019). From these 63 tree-ring width predictors, we developed a nested reconstruction of summer (December through February, DJF) temperature based on partial least squares regression (PLSR). To underscore the efficacy of our approach we provide a comparison with results from the more conventional principal components regression (PCR) approach (e.g., Briffa et al. 1983). To better understand regional summer temperature drivers, and to put our reconstruction into a broader palaeoclimatic context, we analyzed pressure patterns that are responsible for summer temperature variations in the region. Finally, we discussed the new reconstruction, its possible advantages, and its usefulness for the palaeoclimate community.

2 Materials and methods

2.1 Climate of Tierra del Fuego

The climate of most of Patagonia is significantly affected by subtropical anticyclones over the Atlantic and Pacific oceans, whereas the thermal regime in TdF during the whole year is influenced by the Circum-Polar Current and subpolar westerly winds (Jacques-Coper and Bronnimann 2014; Garreaud et al. 2009, 2013). The climate of TdF is of the subpolar oceanic type according to Köppen classification, with cold summer (average temperature (T) around $9\text{ }^{\circ}\text{C}$) and mild winter (average T around $0\text{ }^{\circ}\text{C}$). The southern islands of the archipelago have tundra climate with the mean annual T about $3\text{ }^{\circ}\text{C}$, winter T below $0\text{ }^{\circ}\text{C}$ and annual amplitude of about $5\text{ }^{\circ}\text{C}$ (Paruelo et al. 1998). The amount of precipitation reaches a maximum on the south-west coast (above

1000 mm/year) due to the orographic enhancement by the Andes and reduces to 500–700 mm/year in the south-eastern part and to 300 mm/year in the northern part of the island (Garreaud et al. 2013). Precipitation in TdF falls almost uniformly throughout the year.

2.2 Climate data sets

Climatic data from CRU TS 4.01 archive (Harris et al. 2020; 0.5° resolution) was extracted and averaged for 49 non-empty grid points that cover the study area (73.75°–66.75° W, 53.75°–55.75° S), defined to include the locations of the available chronologies. Monthly values of mean temperature for the whole period 1901–2016 were used, however the longest meteorological record that is situated inside the selected region and contribute to CRU TS starts in 1931 (Ushuaia weather station). Punta Arenas and Punta Dúngenes stations, which both cover the whole period, are situated to the north of this region. However, they contribute to the extracted CRU data due to the interpolation methods used to create the archive based on sparse station locations. A small number of stations may be a problem for reliability of climatic time series in the region, especially for the first third of the twentieth century.

We used geopotential height and wind speed data for 1000 mb, 850 mb, and 500 mb levels from the twentieth Century Reanalysis V3 (Slivinski et al. 2019; 1.0° resolution). Summer (DJF) averages of the SAM were acquired from the reconstruction of Viesbeck (2009), and monthly values based on the methodology of Marshall (2003) were acquired from the British Antarctic Survey (<https://legacy.bas.ac.uk/met/gjma/sam.html>). Monthly values of the Niño 3.4 index (Trenberth and Stepaniak 2001) for the period 1870–2020 based on HadISST (Rayner et al. 2003) that represent ENSO were acquired from the National Oceanic and Atmospheric Administration (NOAA): https://psl.noaa.gov/gcos_wgsp/Timeseries/Data/nino34.long.data.

2.3 Tree-ring data and chronology development

The present study is based on 63 tree-ring width chronologies derived from *Nothofagus pumilio* and *N. betuloides* forests, mainly distributed in the Argentinean sector of Tierra del Fuego, except for seven *N. betuloides* chronologies from the Chilean sector (Fig. 1). The chronologies from the Argentinean sector are the result of several contributions during the last 30 years (Boninsegna et al. 1989; Roig et al. 1996; Roig and Villalba 2008; Massaccesi et al. 2008; Matkovsky et al. 2019). All the 44 chronologies of *N. pumilio*

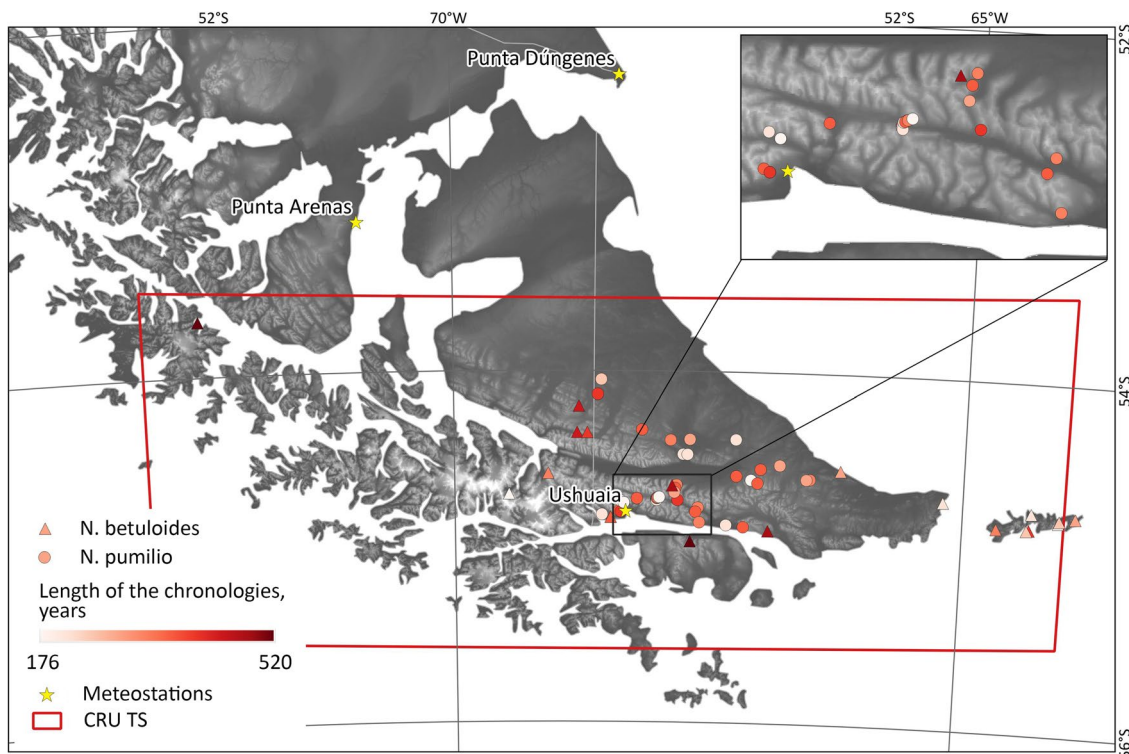


Fig. 1 Map of tree-ring locations used in this study. Colour indicates the length of chronologies. Spatial extent of CRU TS data averaged to get the target variable is marked by red rectangle. Meteorological

stations with the longest records in the region are indicated by stars. Topography is shown in grayscale

used in this study were previously analysed by Matskovsky et al. (2019) for the presence of non-climatically induced seven-year cycles, and these cycles were removed for an enhancement of climatic signal recorded in tree-ring widths. Six chronologies of *N. betuloides* from Chile were described in Fuentes et al. (2019). The longest *N. betuloides* chronology (LRB, 1492–2002, see Table S1, Electronic supplementary material) has been described in Llancabure (2011) and Soto-Rogel and Aravena (2017). The remaining 12 *N. betuloides* chronologies from Argentina were described in Boninsegna et al. (1989) and Roig et al. (2010). Basic statistics on all the chronologies used in the study are shown in Table S1. A kml file with coordinates of all the chronologies is provided in Electronic supplementary material for the possibility of rigorous investigation of their locations. All ring-width measurements were quality checked using the program COFECHA (Holmes 1983; Grissino-Mayer 2001). Tree-ring chronologies were computed using the program ARSTAN (Cook 1985; Cook et al. 2017) by visually controlled application of multiple detrending functions: Huger-shof function, negative exponential, negative or zero-slope straight lines. Indices were computed as the ratios between the original measurements and the fitted curves. Then, for each calendar year, a mean value was computed using a bi-weight robust estimate. No variance stabilization was used. The expressed population signal (EPS), computed in a 30-year moving window with a 29-year overlap, was used to assess how well a finite-sample chronology compares with the theoretical population chronology based on an infinite number of trees (Wigley et al. 1984). For the reconstruction purposes, the commonly used EPS value of 0.85 was used as a threshold to cut the earlier, poorly replicated parts of the chronologies.

2.4 Reconstruction method

2.4.1 Partial least squares regression and principal component regression

To underscore the efficacy of PLSR approach we used for the reconstruction, we provide a comparison with the results from a more conventional PCR approach. We reconstructed summer temperature (dependent variable) from multiple tree-ring chronologies (independent variables) using both methods. Although the physical logic of the process is reversed (the growth of trees depends on the climate parameter, and not vice versa), the problem statement for solving it using data-driven methods uses exactly this formulation—from data to process (Reichstein et al. 2019). PCR is commonly used in dendroclimatology, so we do not describe it in detail. PCR is the base of the Point-by-Point Regression method (PPR, Cook et al. 1999), which is widely used for spatial drought reconstructions based on tree-ring data

(Cook et al. 2015, 2020; Morales et al. 2020). PLSR originated from social sciences but found its broad application mainly in chemometrics (Abdi, 2010). It has also been used in some dendroclimatological studies (e.g. Kalela-Brundin 1999; Timilsena and Piechota 2008; Bauwe et al. 2016), but has not received wide recognition. Both methods help to deal with the problems connected to multicollinearity, which is inevitable in case of highly correlated tree-ring data. Both methods use latent variables, i.e. variables that are inferred from the observed variables through a mathematical model, in this case it is a linear model. A principal difference between PLSR and PCR is that when constructing latent variables (which in the case of PCR are called principal components, PCs) from the initial predictors, the latter method maximizes the explained variance in the set of the predictors, while the former method maximizes the explained variance in the dependent variable. In other words, PCR decomposes \mathbf{X} in order to obtain components which best explains \mathbf{X} . By contrast, PLS regression finds components from \mathbf{X} that best predict \mathbf{Y} , where \mathbf{X} and \mathbf{Y} are the matrices of independent and dependent variables correspondingly. For a detailed mathematical description of PLSR please refer to Abdi (2010) and references therein.

We tested how the performance of the PLSR and PCR methods changes depending on the number of predictors and latent variables. We used the coefficient of determination (R^2) on cross-validation to evaluate the methods' performance and to overcome possible overfitting. The cross-validation workflow consisted of multiple iterations where k -fold cross-validation with k running from 2 to 6 was repeated 10 times each. The data withheld from the calibration were used for calculation of R^2 . To address performance of the methods with different number of predictors and different number of latent variables, we randomly selected specified number of predictors from the full data set and calculated R^2 for different numbers of latent variables from 1 to the number of selected predictors. To reduce dependence of the results from specific sets of good or bad predictors, we made 50 repetitions with random subsets of predictors for each number of predictors and each number of selected latent variables. The workflow is described in detail in the Electronic supplementary materials Sect. 1.

When using methods which utilize latent variables, such as PCR and PLSR, a question of selection of the appropriate number of latent variables emerges. In contrast to PCR, in PLSR latent variables are sorted in the order of decreasing explained variance of the dependent variable. Hence, in PLSR the cumulative explained variance increases steadily with the addition of latent variables. In PCR it increases irregularly, with significant spikes on adding a principal component (PC) which explains a significant amount of variance of the dependent variable. At the same time, when using PLSR it is especially important to use cross-validation,

as it is strongly subjected to overfitting due to its ability to adjust to the target variable (Geladi and Kowalski 1986; Abdi 2010). In our study we used cross-validation to select the appropriate number of latent variables. This experiment as a whole may be considered as a theoretical example of one step of point-by-point regression (PPR), tested with real data for TdF archipelago.

2.4.2 Nested reconstruction approach

To get advantages of both the number of chronologies and the lengths of the longest ones, we used a nested reconstruction approach (Meko 1997). In this approach, different parts of the reconstruction are produced using different sets of chronologies. Thus, each part of the reconstruction has different calibration and validation statistics, with the quality usually decreasing back in time. In this way we, on the one hand, provide the maximum reasonable length of the reconstruction, and, on the other hand, provide the maximum reconstruction skill for each period. Statistics r , R^2 on calibration and R^2 on cross-validation were used to describe the skill of each part of the reconstruction (see Electronic supplementary materials Sect. 1 for details). In the paper by the term “variance explained by the reconstruction” we mean the values of R^2 on cross-validation over the instrumental period.

To select the target variable for the reconstruction we were guided by a set of considerations. First, it was previously demonstrated, that air temperature for different summer months is the main driver of tree growth in the region, with the highest correlations in December for *N. pumilio* chronologies and in January for *N. betuloides* chronologies (Massacessi et al. 2008; Matskovsky et al. 2019; Fuentes et al. 2019). Second, DJF temperatures has been widely used in multiple climatological and paleoclimatological studies, including modelling. Hence, this target variable was preferred for compatibility with other studies. Third, in our experiments with different target variables we found that mean DJF temperature was one of the best performing targets for our data set.

To select the predictors, different sets of tree-ring chronologies were tested. We used a manual analogue of stepwise regression, adding and removing predictors to find the best subset.

To quantify the uncertainties associated with the reconstruction, we produced multiple reconstructions based on reduced the number of chronologies in each nest and reduced length of the calibration period. We removed 0 to 2 chronologies from each nest and reduced the length of the calibration period to 50–90% of the full length. These changes were randomly generated and iterated, all together 35,650 times. Each time a reconstruction has been produced. The estimated uncertainties are hence attributed to the amount

of available proxy data (exclusion of the chronologies) and to the availability and reliability of the instrumental data (reduction of the calibration period).

We used ‘Extreme Value Capture’ (EVC) test (McCarroll et al. 2015) to measure how well our reconstruction captures the extreme values of the instrumental data. EVC test is a statistical test based on the binomial distribution. We used the following parameters of the binomial distribution: $n = 10$ (the number of selected extreme years) and $p = 0.098$ ($p = 10/102$ is the probability for each of 102 years of the common period AD 1901–2002 to be one of 10 extreme years). Ten maxima and ten minima were tested separately.

3 Results

3.1 Summer temperature reconstruction in Tierra del Fuego since CE 1765

The final reconstruction (Fig. 2) was derived for the target variable of summer (DJF) air temperatures using PLSR and a nested reconstruction approach. The advantage of PLSR over PCR is demonstrated in the Electronic supplementary materials Sect. 2. In Fig. 3, all individual PLSR reconstructions (nests) are shown, and their performance is described in Table 1. In each nest a cutoff of four latent variables has been finally used. With a reduced number of available and well-replicated chronologies, the skill of the reconstruction reduces back in time. Almost 50% of variance is explained for the best-replicated part (1889–2002), and 37% of the variance is explained by the nest representing the oldest part of the reconstruction (1765–1853). Nevertheless, the whole reconstruction evidence positive skill, providing valuable information about summer temperature variations in the past.

The recent part of the reconstruction agrees with the instrumental data very well, including high- and low-frequency variations (Fig. 2a, b). The most prominent agreement is seen for the first half of the twentieth century, while in the second half we see a divergence, including the cold peak of 1970–1971 which is not adequately reproduced by the reconstruction. This divergence is in line with the finding of decreased temperature signal in tree-ring widths of *N. pumilio* in TdF since 1970s (Matskovsky et al. 2019). Using EVC we assessed the probabilities that 10 minimum and 10 maximum years of our reconstruction for the instrumental period correspond to those of the instrumental data. For the maxima we have coincidence in 5 of 10 years (1902, 1903, 1904, 1918, 1919; $p = 0.0014$, highly significant). For the minima we have coincidence in 3 of 10 years (1934, 1955, 1960; $p = 0.055$, insignificant). Two additional minima do not coincide but are close (1908 and 1947 in the reconstruction and 1909 and 1946 in the instrumental data). The

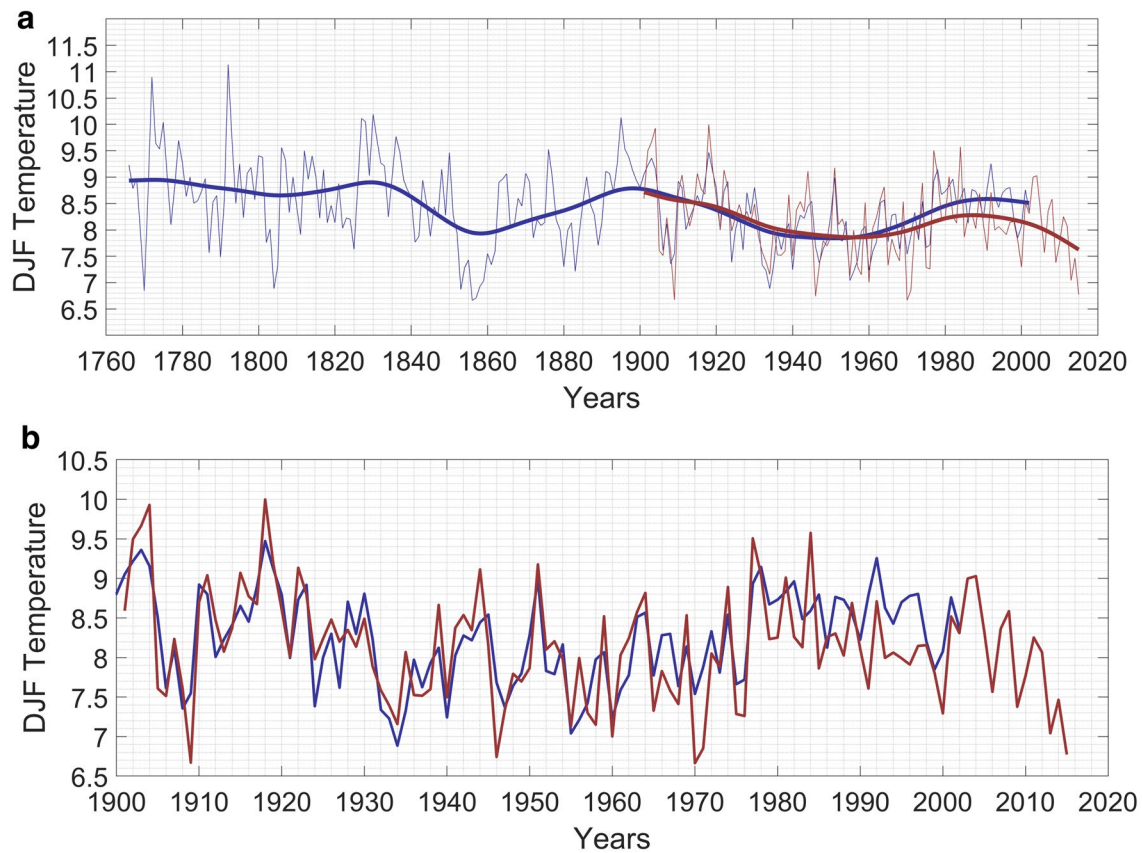


Fig. 2 Comparison of the instrumental (red) and reconstructed (blue) DJF temperatures in Tierra del Fuego. **a** Full period. **b** Instrumental period. Series smoothed with 50-yr spline are shown with thick lines

reconstruction follows the instrumental data very well, with all the warm peaks represented and having comparable values. Minima are represented worse. Low-frequency variations of the instrumental temperature are well preserved by the reconstruction (Fig. 2a), despite different autocorrelation structure of the two time series: for the instrumental data, lag-one autocorrelation coefficient (AC1) is 0.31, while for the reconstruction AC1 is 0.55. Good correspondence of instrumental and reconstructed time series in the first third of the twentieth century increase our confidence in the reliability of the instrumental data for this period. Large spatial extent of the tree-ring data and relative spatial homogeneity of summer temperature in TdF may be the reasons for such correspondence.

The reconstruction indicates more than a century-long warm period between 1765 and 1905, with short cold interruptions in 1800s, 1850s–beginning of 1860s, and 1880s. The ten-year period 1853–1862 was unprecedentedly cold over more than 250 years of the reconstruction, but the period 1932–1976 covered by the instrumental data was a longer period with the temperatures below average.

Figure 3 gives an opportunity to explore the similarities and differences of the individual reconstructions (nests), as

well as uncertainties of the reconstruction. Even those parts that include chronologies with EPS values lower than 0.85, and therefore were excluded from the final reconstruction, are in a good agreement, especially throughout the nineteenth century. This fact increases our confidence in the reconstruction for this period. The spread among the reconstructions is higher during the transition from the 18th to nineteenth century (1780–1840). For this period, the reconstructions that demonstrate higher explained variance over the instrumental period, indicate lower temperatures. However, these ‘colder’ reconstructions are of less confidence because of low sample replication and low EPS values. At the same time, the longest nest (and the less skilful one) shows rather good agreement with the other nests, especially at lower frequencies. Altogether, the intercomparison of the individual reconstruction nests reaffirms credibility of the nested reconstruction approach used in this study.

3.2 Observed summer temperature variations in Tierra del Fuego and its drivers

Having the new reconstruction in hand, we want to understand the drivers of summer temperature variations in the

Fig. 3 a. Individual reconstructions that were joined to produce the final nested reconstruction. The instrumental data is shown in black. Each reconstruction is shown with the colour corresponding to the explained variance of the instrumental data (see colour bar). Before the EPS > 0.85 cut off the reconstructions are shown semi-transparent. The fourth reconstruction (green, based on BRI, VAL, LRB, DP, and DF2 chronologies) has not been included into final reconstruction, as it increases its length only for 10 years, while has significant reduction in skill (28% of variance explained compared to the next nest with 37% of variance explained). It is shown to demonstrate the degree of covariance of the reconstructions based on different subsets of chronologies. **b.** Uncertainties associated with the reconstruction. The final reconstruction is shown in red; uncertainties are shown as grey shading

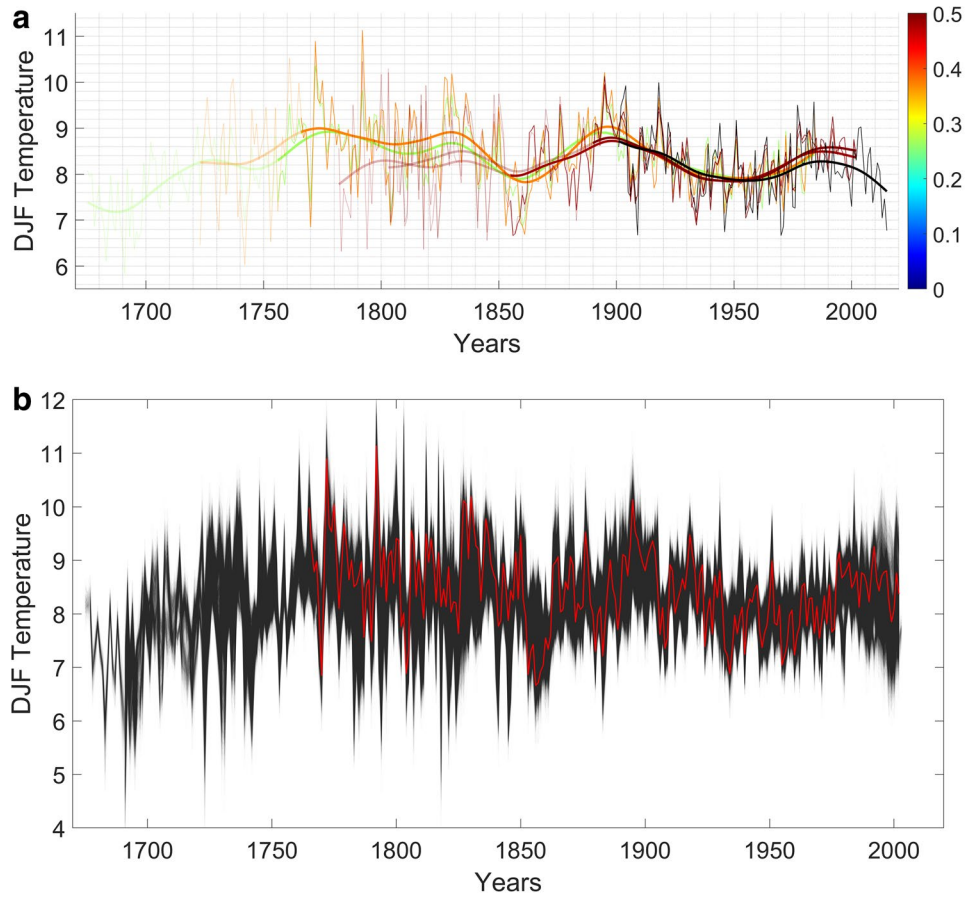


Table 1 Description of the reconstruction nests

Common period of the chronologies used	Chronologies used (number)	Correlation with the target variable	R ² on calibration	R ² on cross-validation	MIN EPS > 0.85	Period covered by each nest in the final reconstruction
1803–2002	CUC, GUA, KRS, KR8 , MBR, PAR, PG, VAH, LRB (10)	0.790	0.624	0.498	1776, 1796, 1760, 1839, 1889 , 1759, 1854, 1766, 1844, 1600	1889–2002
1782–2002	CUC, GUA, KRS, KR4, MBR, PAR , PG, VAH, LRB (9)	0.771	0.595	0.482	1776, 1796, 1760, 1839, 1759, 1854 , 1766, 1844, 1600	1854–1888
1723–1985	BRI, ESJ , OBS, VAL, LRB, DP, DF2 (7)	0.706	0.498	0.373	1727, 1765 , 1716, 1751, 1600, 1754, 1755	1765–1853

Bold text shows the chronology and the year which limit each reconstruction nest based on EPS > 0.85 criterium. The R² statistics are calculated for the maximum period of overlap between each nest and instrumental period

region. If the regional summer temperature variations are strongly connected to the major Southern Hemisphere indices, we may use the reconstruction for some inferences about hemispheric processes. If they are driven by other modes of atmospheric variability, we may take advantage of the discrepancies between our reconstruction and reconstructions from the nearby and remote regions to study intrinsic

regional variability. The analysis provided below is aimed to address this bifurcation.

Although climate in southern South America is strongly influenced by large-scale atmospheric systems in the Southern Hemisphere (Garreaud et al. 2009, 2013), we found that observed summer temperature in TdF was weakly connected to major Southern Hemisphere indices. There

were no significant correlations neither with summer SAM ($r = -0.10$, $p = 0.3$, 1901–2005; $r = 0.01$, $p = 0.94$ 1957–2016), nor with summer ENSO 3.4 ($r = 0.08$, $p = 0.39$, 1901–2016). Hence, we expected other modes of atmospheric circulation variability to be responsible for summer temperature oscillations in TdF.

We explored specific patterns of atmospheric circulation related to positive and negative monthly temperature anomalies in austral summer (Fig. 4). Circulation pattern for positive temperature anomalies larger than 1°C (Fig. 4a, b, red isolines) shows dominance of an active low-pressure centre to the west of Antarctic Peninsula (mostly pronounced in December) and a high-pressure ridge near the east coast of Patagonia (which is stretched to Antarctic Peninsula in

February). This system enhances the meridional circulation and promotes the advection of warm northern air masses into TdF. For the years with negative summer temperature anomalies with absolute values greater than 1°C (Fig. 4a, b, blue isolines), the atmospheric circulation pattern shows dominance of a cyclonic activity near the Weddell Sea, which probably strengthens the westerlies and produces the south-west cold air advection into TdF. These two patterns of pressure systems for positive and negative summer temperatures in Southern South America were also discussed in Alessandro (2008).

According to the average wind speed data for the 1901–2015 period, during summer (DJF) the climate of TdF is affected by the westerly winds (Fig. 4a–c). However,

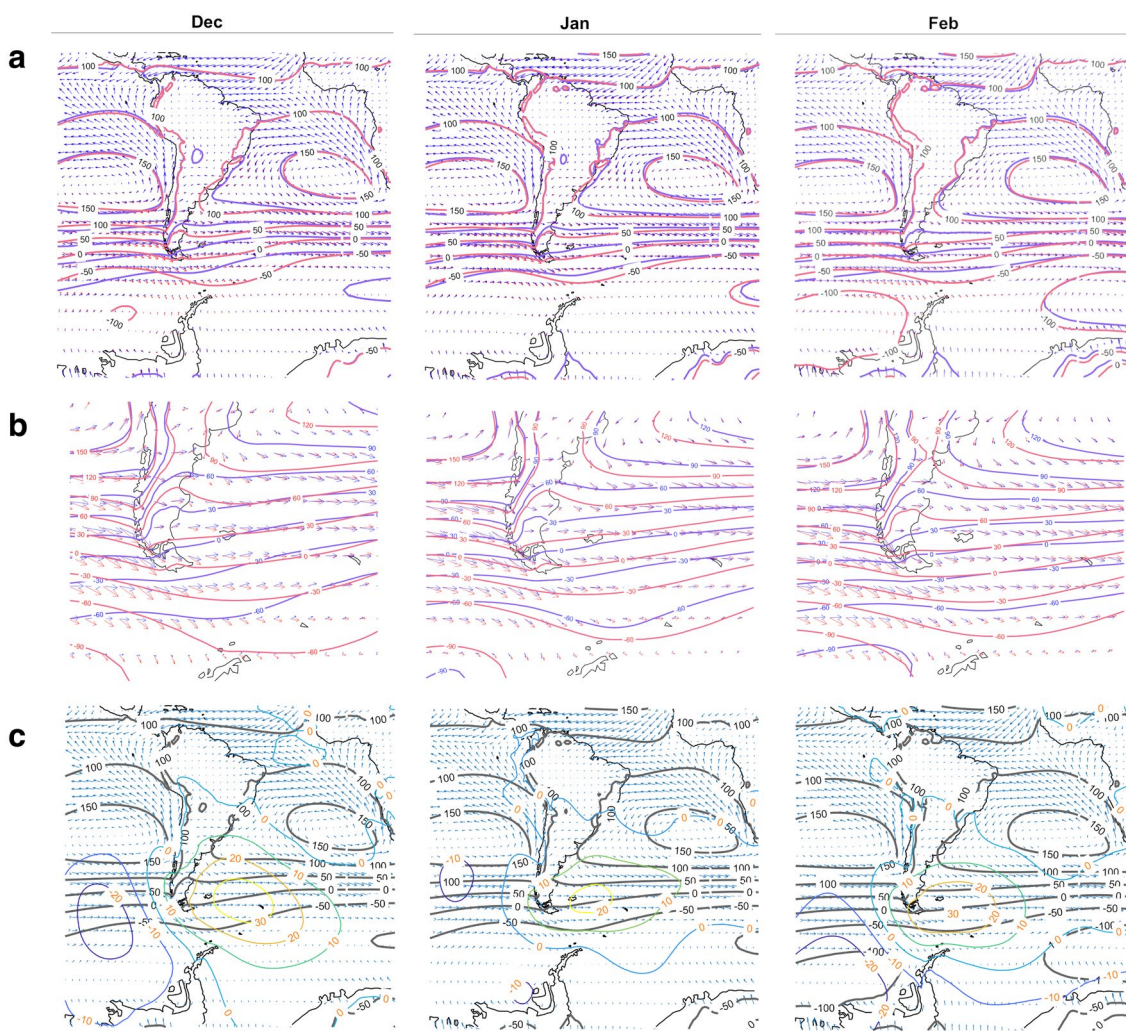


Fig. 4 Meteorological processes affecting summer temperature in Tierra del Fuego for the period of 1901–2015. **a** Average circulation patterns for positive (reddish colour) and negative (bluish colour) summer temperature anomalies in Tierra del Fuego for the period between 1901 and 2015 (from 20th Century Reanalysis V3). Contour lines show geopotential height at 1000 mb level. Arrows show wind

speed at 1000 mb level. **b** are the **a** panels zoomed in. **c** Grey contour lines show average geopotential height at 1000 mb level. Coloured contour lines show geopotential differences for the years with positive and negative temperature anomalies. Blue arrows show wind speed at 1000 mb level

there is a difference in geopotential heights between years with positive and negative temperature anomalies (Fig. 4c). These anomalies represent an anticyclone in the Southern Atlantic with the centre between Malvinas and South Georgia Island. Another anomaly forms a cyclone in the Southern Pacific with the centre migrating from north to south at the longitude of approximately 100°W. These processes are not actual synoptic processes but rather an average of pressure anomalies for many years. However, this atmospheric dipole explains rather well the variability of summer temperatures in TdF. Correlations of regional monthly temperatures with 850 mb geopotential heights reach $r=0.73$ ($p<0.001$) in the centre of this anticyclone and have significant negative values (up to $r=-0.4$, $p<0.001$) in the cyclone (Fig. 5c). Wind vectors show that during warm temperature anomalies the intensity and frequency of northern winds in TdF increase (Fig. 5a, c). The described dipole system was found to be more intensive in December and February, than in January, and there is a difference in the positions of negative pressure anomalies for different months (Fig. 5).

The geopotential height and wind anomaly composite fields for temperature anomalies greater than 1 °C (Fig. 5a)

confirm that in December and January the pressure centre that drives positive temperature anomalies is a part of the quasi-stationary wave train with a quasi-barotropic structure extending from Australia across the South Pacific and ending with a cyclonic circulation centre in the South Atlantic Convergence Zone (SACZ). In February, the wave train appears to extend less westward, spreading over the adjacencies of southern South America and the Antarctic Peninsula. Conversely, negative temperature anomalies in TdF are associated with geopotential height anomalies of inverse sign to those of the positive temperature anomalies (Fig. 5b). An anomalous low-pressure centre is located over the Southern Atlantic ocean affecting the TdF region with enhanced southern circulation. This centre is also a part of the wave train that extends along the Pacific ending in the SACZ. For all the summer months it is extended in a more zonal form towards the Indian Ocean.

Based on these results, we argue that regional oscillations of large-scale pressure systems forming on the way of Southern Hemisphere subpolar westerly winds affect summer temperature variability in TdF. The sign and intensity of summer temperature anomalies depend on the existence

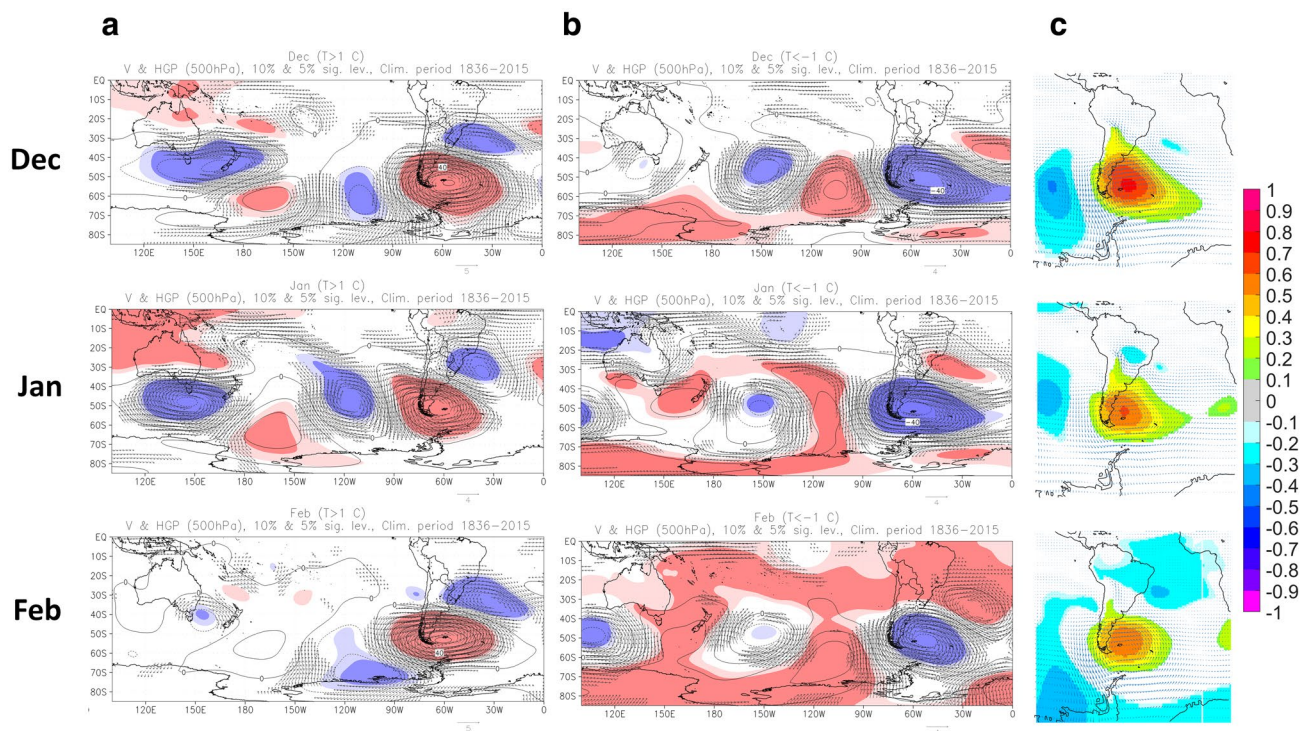


Fig. 5 a Composite fields of geopotential height and wind anomalies for years with temperature anomalies > 1 °C in Tierra del Fuego, corresponding to December (top), January (centre) and February (bottom), at the 500 hPa level. The shaded areas correspond to significant anomaly values at ($p < 0.1$) (light) and ($p < 0.05$) (dark) levels (positive in red, negative in blue). Only wind vectors when at least one component, u or v, is significant at the ($p < 0.05$) level are plot-

ted. **b** Idem **a** but for temperature anomalies < -1 °C in Tierra del Fuego. **c** Correlation coefficients between temperature in Tierra del Fuego and geopotential height at 850 mb level. Only significant values are shown ($p < 0.05$). Blue arrows show wind speed differences at 850 mb level for the years with positive and negative temperature anomalies

and intensity of the atmospheric dipole and the storm tracks in the South Atlantic and South Pacific. We discuss these results in the following section to provide a broader context for interpretations of our new reconstruction.

4 Discussion

4.1 Local vs hemispheric drivers of summer temperature variations in Tierra del Fuego

According to our results, the direct influence of large-scale atmospheric patterns (SAM and ENSO) on the variations of summer temperature in TdF is limited. These results are in agreement with previous works (Soto-Rogel and Aravena 2017; Fuentes et al. 2019) and highlight the importance of mesoscale and synoptic scale atmospheric processes in the region. It is unclear at this stage whether concomitant effects of ENSO and SAM (Fogt and Bromwich 2006) in the study area can be detected for surface summer temperatures within longer time scales as pointed out by Dätwyler et al. (2020). It is known that geopotential high at centres of action such as the area of the Ross and Bellingshausen seas and the Weddell sea are of importance for the modulation of the advection over Southern South America.

Jacques-Coper et al. (2016) have indicated that summer heatwaves in Patagonia (46–52°S, 201 cases were analysed) usually form when an anticyclone exists in the Atlantic Ocean near the east coast of Patagonia, which causes the northern warm advection. The authors showed that this anticyclone begins to form near the west coast of TdF and moves further to the north-east. Analysing 500 mb geopotential heights composites fields the authors have observed that this high-pressure centre forms within the large-scale baroclinic wave system over the South Pacific. This process begins from the formation of a low-pressure anomaly near the south-east coast of Australia and develops over a period of 21 days throughout the South Pacific. Here we showed that the pressure dipole that is associated with summer temperature anomalies in TdF (Fig. 4c) is a part of a similar large-scale pressure wave pattern (Fig. 5a, b).

Garreaud et al. (2013) highlighted that the stronger westerlies cause cooler summers at the southern part of South America. Besides, Alessandro (2008) showed that cold summer T anomalies occur in TdF when the trough at 500 mb level is situated over the Antarctic Peninsula or moves to the east and is centred over the Weddell Sea, producing the south-western cold advection. Thus, the positive summer T anomalies in TdF apparently are consequences of high-pressure anomaly to the east of Patagonia, which corresponds to a ridge in the region at high altitudes. As T anomalies in TdF relate to the variations

in storm tracks in South Pacific and South Atlantic, negative T anomalies occur when the storm tracks move to the north, enhancing the cyclonic activity southeast of TdF.

Several works (Jacques-Coper and Bronnimann 2014; Jacques-Coper and Garreaud 2015) disclosed the shift in South American climate since the end of 1970s, when the intensification of the Atlantic subtropical anticyclone occurred, and the westerlies zone moved south. These processes probably caused divergent trends in winter and summer temperatures in Southern Patagonia after the year 1980, which are clear in the observed data (Fig. S4a, b, Electronic supplementary material). Negative temperature trend in TdF summer temperature since early 1980s also diverges from positive trend in South America and Southern Hemisphere summer temperature throughout the same period. This shift is also obvious in the instrumental DJF temperature as a significant rise from 1976 to 1977. Our reconstruction represents well this shift; however, it is not so good in representing subsequent declining trend until 2000. Reduced quality of the reconstruction since 1970s is probably caused by reduced climatic sensitivity of the trees during this period (Matskovsky et al., 2019). One of the possible reasons for the reduced climatic sensitivity of the trees is the discussed climatic shift of the late 1970s.

4.2 PLSR as a substitute to PCR in tree-ring-based climate reconstructions

Our data set includes chronologies derived from two tree species (*N. pumilio* and *N. betuloides*) growing in sites with different conditions, including altitude, exposition, soils, etc. According to previous studies (Massaccesi et al. 2008; Matskovsky et al. 2019; Fuentes et al. 2019) there are different patterns of climatic response of the two studied species in the region: *N. pumilio* has temperature response shifted to the end of spring—beginning of summer (November, December), while the temperature response of *N. betuloides* is shifted towards the end of summer—beginning of autumn (January, February, March). The best reconstruction results we acquired for the sets of predictors that included both species, hence pointing on the potential ability of the reconstruction method to extract information about different periods of the summer season from the chronologies of different species. Remarkably, the values of R^2 on cross-validation as high as 0.5 were acquired from a set of predictors none of which has correlation with the target variable higher than $r=0.38$, and some having negative correlations.

Stability of climate-to-proxy relationships is another concern when reconstructing past climates, and especially when complex dependencies including many predictors are considered. In our case, similarity of different reconstructions based on different sets of chronologies (Fig. 3), including

low-frequency variability, is an indirect confirmation of the stability of discovered relationships. Another confirmation is that all the reconstruction nests passed cross-validation tests and showed positive R^2 values on the data withheld from calibration (Table 1).

Concerning the methods for the extraction of climatic information from tree rings, here we considered two of them—PCR and PLSR. The difference between PLSR and PCR is that the former method constructs components to maximize the explained variance in the target variable, while the latter maximizes it in the matrix of predictors. Such a modeling approach implemented in PLSR seems reasonable in case of dendroclimatic reconstructions based on multiple chronologies, since it allows to extract common information related to the target climatic variable from the set of chronologies, and not to extract common signal first, as is the case when using the PCR method. Hence, PLSR usually needs less latent variables to reach the same amount of explained variance. Speaking in common dendroclimatic terms, we can consider PLSR to be a better filter that separates signal from noise. By the term “signal” here we consider the target climate variable, differently to a common dendroclimatic understanding of signal as a common variance of tree-ring chronologies. In the case of PLSR, the signal is kept in the first few latent variables, and the noise is distributed with the others. Better separation of signal from noise by PLSR is confirmed by higher cross-validation statistics in comparison with PCR (Fig. S1, Electronic supplementary material).

As we have seen in the results (Sect. 3.2, Fig. S3 of the Electronic supplementary material), in the case of PCR some important information was contained in the principal components of lower order. Conversely, in the case of PLSR explained variance increased rapidly for the first latent variables, and then the increase decelerates. Such a property of PLSR makes it easy to fix the necessary number of latent

variables to keep, which is especially important for an automated processing of large data sets, for instance in the PPR method.

In our case, PLSR extracted climatic information from a set of tree-ring predictors better than PCR. The explanation of this result may be the following: some of the trees growing in specific conditions provide useful information that is different from the information from other locations. PCR which extracts common information from tree-ring predictors will leave important but individual information about climatic signal from certain sites in the components of lower order. The reconstruction consequently loses this information if those components are omitted. Hence, different screening procedures aimed at the reduction of quantity of predictors may lead to the loss of important climatic signal in the final reconstruction. In an automated setting where rigorous selection of predictors is impossible, PLSR may show improvement over PCR, using less latent variables at the same time. To sum it up, our results show advantages for substitution of PCR for PLSR in an automated setting like PPR. However, our experiments were performed for a specific region and one data set, and additional tests from other different environments are required to confirm this finding.

4.3 Comparison with other regional temperature reconstructions

We compared our summer temperature reconstruction for TdF with other temperature reconstructions for TdF and Southern Patagonia. Such a comparison is necessary to place the new reconstruction into the paleoclimatic context of the region and to define its most reliable periods and timescales. In this work we have updated and incorporated many of the existing tree-ring chronologies in the area. Thus, certain similarities among the data sets used in this

Fig. 6 Comparison of various temperature reconstructions for Tierra del Fuego and Southern Patagonia. All the reconstructions are standardized to have the same mean and standard deviation for the period AD 1901–1983. Thin lines are annual values, thick lines are 50-year smoothing splines

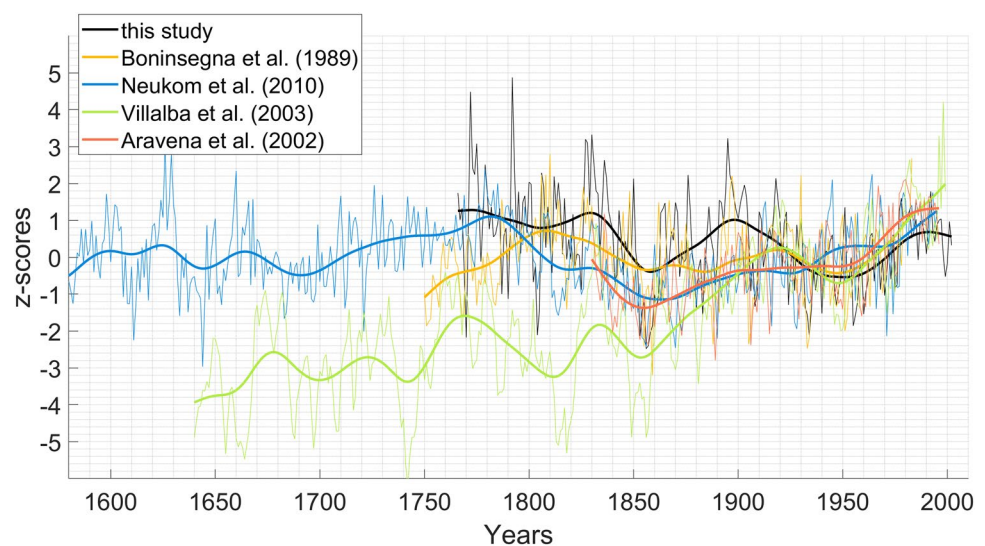


Table 2 Correlation coefficients of various temperature reconstructions for Tierra del Fuego and Southern Patagonia for the common period AD 1830–1983

	This study, TdF DJF temp	B89, Ushuaia NDJF temp	N11 South patagonia DJF temp	V03 Southern sector of Southern andes, mean annual temp	A02 Punta arenas minimum annual temp
This study	1	0.33	0.10	0.21	0.38
B89	0.36	1	0.12	0.21	0.21
N11	0.20	0.08	1	0.49	0.48
V03	0.42	0.18	0.33	1	0.53
A02	0.58	0.18	0.34	0.32	1

Values above the main diagonal were calculated for the initial reconstructions, values below the diagonal were calculated for detrended reconstructions

and previous studies are unavoidable. The reconstructions used for the comparison include a NDJF reconstruction of Ushuaia temperature (Boninsegna et al. 1989), a DJF temperature reconstruction for Southern Patagonia (Neukom et al. 2011), a mean annual temperature reconstruction for the southern sector of the southern Andes (Villalba et al. 2003), and a reconstruction of minimum annual temperature of Punta Arenas (Aravena et al. 2002), hereafter referred to as B89, N11, V03 and A02 respectively (Fig. 6, Table 2). All but N11 are based solely on tree-ring data, while N11 is a multi-proxy reconstruction. All reconstructions except B89 are produced for different regions, while B89 tree-ring data are acquired from the same region as our reconstruction, and have many sites in common. All reconstructions except N11 have different target seasons compared to our reconstruction. To explore the differences in target variables, the different temperature targets for different regions are plotted for the instrumental period (Fig. S4, Electronic supplementary material). Some of the differences between the reconstructions are due to different target seasons or regions, however certain similarities of the reconstructions are also obvious. These similarities indicate the most prominent and reliable paleoclimatic shifts in TdF and Southern Patagonia. One of the most obvious similarities is the pronounced cold period lasting almost a decade in the 1850s. Other common features include relatively warm periods in 1760s–90s (except B89), 1820s–30s, and 1910s.

To assess quantitative measure of similarity for the compared reconstructions, we calculated correlation coefficients between these reconstructions for the common period 1830–1983 (Table 2). Our reconstruction has the strongest correlation with A02 ($r=0.38$). To compare the reconstructions at higher frequencies and to eliminate the effect of long-term trends, which may arise from data treatment, we also considered correlations between the detrended (subtracted linear trend) reconstructions. Correlations with detrended reconstructions increase, reaching the highest values of $r=0.58$ and $r=0.42$ for A02 and V03 respectively. We consider detrended data because some reconstructions based on tree-ring data may

have spurious trends connected to detrending procedures and sampling biases (Briffa and Melvin 2011). For example, V03 reconstruction may contain a trend arising from ‘Modern-sample’ bias (Briffa and Melvin 2011, their Fig. 5.6) due to application of the Regional Curve Standardization (RCS) method to a sample consisting of living trees solely, without inclusion of any subfossil trees. Without this trend, which is probably artificial, V03 would align much better with our reconstruction. However, the question of actual low-frequency temperature variations, including trends for the last 250 years, remains open. Our reconstruction is limited in its ability to reproduce climatic trends on the timescales approaching the mean age of the trees due to the individual detrending approach we used to standardize the tree-ring series (Cook et al. 1995). At the same time, reconstructed temperature variations at periods up to 150–200 years long should be reliable due to mean length of tree-ring series used for the reconstruction. Improvement in reconstruction of low-frequency climatic variations using chronologies based on living trees only may be achieved by application of signal-free standardization (Melvin and Briffa 2008) in combination with single-series detrending (Supplementary materials for Cook et al. 2015).

The reconstructions N11, V03 and A02 showed high values of pairwise correlation coefficients (ranging from 0.48 to 0.53, Table 2) first due to common trends (correlation coefficients for detrended reconstructions are lower, ranging from 0.32 to 0.34) and second because of the presence of common predictors, since N11 includes tree-ring data used in V03 and A02.

The differences between our and the other reconstructions (N11 and V03) are especially evident for the earlier part, particularly for the period between 1765 and 1850. Exceptionally high reconstructed values that are represented in our reconstruction in the 1770s and 1791 are not present in the other considered reconstructions. These discrepancies might be due to regional differences, as N11 and V03 represent continental part of the Southern Patagonia. Hence, our new reconstruction provides new paleoclimatic

evidence for TdF which was not previously available from other reconstructions.

5 Conclusions

- We developed a new summer temperature reconstruction for Tierra del Fuego covering the period 1765–2002. It explains 37–50% of instrumental temperature variability. The reconstruction provides a new paleoclimatic record for the region with sparse high-resolution temperature archives. It has a remarkably high reconstruction skill, especially given the generally moderate climatic signal contained in tree-ring widths in the region.
- Summer temperature variability in Tierra del Fuego is primarily driven by the fluctuations of atmospheric pressure systems both in the South Atlantic and South Pacific near the coast of Tierra del Fuego. At the same time, it is insignificantly correlated to the major hemispheric modes: ENSO and SAM. Hence, the new reconstruction reveals intrinsic regional variability, the fact that makes it especially important for climate modelling experiments. Our reconstruction can be used for direct comparison with model outputs to better understand model limitations or to tune a model. It can also contribute to larger scale reconstructions based on paleoclimatic data assimilation.
- The pressure system that drives summer temperature variability in TdF is a part of quasi-stationary wave train with a quasi-barotropic structure extending across the South Pacific.
- PLSR showed improved performance over PCR in the case of multiple tree-ring predictors without pre-screening. According to these results, PLSR may be a preferable method over PCR for the use in automated tree-ring based reconstruction approaches, akin widely used point-by-point regression. However, the performance of PLSR should be additionally tested on multiple data sets from different environments.
- Due to its location in a remote and poorly studied region, common target variable, high explained variance, and described relationship of the target variable with the regional atmospheric processes, the new reconstruction is a unique and especially valuable source for the paleoclimatic community, including climate modellers.

Supplementary Information The online version contains supplementary material available at <https://doi.org/10.1007/s00382-022-06384-0>.

Acknowledgements We are grateful to anonymous reviewers whose comments helped to improve the quality of the manuscript. VM acknowledges CONICET for a postdoctoral fellowship that partly supported this study. The first authors wish to thank Guillermo Martínez

Pastur, Claudio A. Roig, Juan Andrés Miller, Polina Morozova, Yamina Micaela Rosas and Ricardo Vukasovic for their help during fieldwork. José Boninsenga, Juan Carlos Llancabure and other contributors of tree-ring chronologies from Tierra del Fuego are highly acknowledged. Fieldwork in Argentina was partly supported by the Russian State Assignment Project FMGE-2019-0004 (AAAA-A19-119022190172-5). Assessment of performance of different reconstruction methods was supported by the Russian Science Foundation grant no. 21-17-00264. This is a contribution to the project PUE-0091/2016-CONICET. The study was completed in the laboratory created by Megagrant project (agreement no. 075-15-2021-599, 08.06.2021).

Funding The funding has been received from Russian Science Foundation with Grant no. 21-17-00264; Ministry of Education and Science of the Russian Federation with Grant no. FMGE-2019-0004; МЕГАГРАНТЫ with Grant no. 075-15-2021-599; Consejo Nacional de Investigaciones Científicas y Técnicas with Grant no. PUE-0091/2016-CONICET.

Data availability The data sets analysed in the current study are available from the corresponding author on reasonable request after consultation with the other authors who were responsible for the generation of the data sets.

Declarations

Conflict of interest The authors have no conflicts of interest to declare that are relevant to the content of this article.

References

- Abdi H (2010) Partial least squares regression and projection on latent structure regression (PLS Regression). Wiley Interdiscip Rev Comput Stat. <https://doi.org/10.1002/wics.51>
- Alessandro AP (2008) Temperature and precipitation conditions in Argentina associated with strong westerly mid-latitude. Rev Bras Meteorol. <https://doi.org/10.1590/s0102-77862008000200002>
- Aravena JC, Lara A, Wolodarsky-Franke A, Villalba R, Cuq E (2002) Tree-ring growth patterns and temperature reconstruction from *Nothofagus pumilio* (Fagaceae) forests at the upper tree line of southern Chilean Patagonia. Rev Chil Hist Nat. <https://doi.org/10.4067/S0716-078X2002000200008>
- Bauwe A, Jurasinski G, Scharnweber T et al (2016) Impact of climate change on tree-ring growth of scots pine, common beech and pedunculate Oak in northeastern Germany. Iforest 9:1–11. <https://doi.org/10.3832/ifor1421-008>
- Boninsegna JA, Keegan J, Jacoby GC, et al (1989) Dendrochronological studies in Tierra del Fuego, Argentina. In: Quaternary of South America and Antarctic Peninsula. pp 305–326
- Boninsegna JA, Argollo J, Aravena JC et al (2009) Dendroclimato-logical reconstructions in South America: a review. Palaeogeogr Palaeoclimatol Palaeoecol 281:210–228. <https://doi.org/10.1016/j.palaeo.2009.07.020>
- Briffa KR, Jones PD, Wigley TML, Pilcher JR, Baillie MGL (1983) Climate reconstruction from tree rings: Part 1, basic methodology and preliminary results for England. J Climatol 3(3):233–242
- Briffa KR, Melvin TM (2011) A closer look at regional curve standardization of tree-ring records: In: Justification of the need, a warning of some pitfalls, and suggested improvements in its application

- Cook ER, Briffa KR, Meko DM, Graybill DA, Funkhouser G (1995) The 'segment length curse' in long tree-ring chronology development for palaeoclimatic studies. *Holocene* 5(2):229–237
- Cook ER, Meko DM, Stahle DW, Cleaveland MK (1999) Drought reconstructions for the continental United States. *J Clim* 12:1145–1163
- Cook ER, Seager R, Kushnir Y et al (2015) Old World megadroughts and pluvials during the Common Era. *Sci Adv*. <https://doi.org/10.1126/sciadv.1500561>
- Cook ER (1985) A Time series analysis approach to tree ring standardization (dendrochronology, forestry, dendroclimatology, autoregressive process). *Sch Renew Nat Resour*.
- Cook ER, Krusic PJ, Peters K, Holmes RL (2017) Program ARSTAN version 48d2, autoregressive tree-ring standardization program. Tree-Ring Laboratory of Lamont-Doherty Earth Observatory. <http://www.ldeo.columbia.edu/tree-ringlaboratory/resources/software>.
- Cook ER, Solomina O, Matskovsky V et al (2020) The European Russia drought atlas (1400–2016 CE). *Clim Dyn*. <https://doi.org/10.1007/s00382-019-05115-2>
- Dätwyler C, Grosjean M, Steiger NJ, Neukom R (2020) Teleconnections and relationship between the El Niño-Southern Oscillation (ENSO) and the Southern Annular Mode (SAM) in reconstructions and models over the past millennium. *Clim Past*. <https://doi.org/10.5194/cp-16-743-2020>
- Fogt RL, Bromwich DH (2006) Decadal variability of the ENSO teleconnection to the high-latitude south pacific governed by coupling with the Southern Annular mode. *J Clim*. <https://doi.org/10.1175/JCLI3671.1>
- Franco MG, Mundo IA, Pastur GJM, Barrera MD (2019) Radial growth responses to thinning and climate in native *Nothofagus betuloides* forests in Tierra del Fuego, Argentina. *Dendrochronol* 57:125625
- Fuentes M, Aravena JC, Seim A, Linderholm HW (2019) Assessing the dendroclimatic potential of *Nothofagus betuloides* (Magellan's beech) forests in the southernmost Chilean Patagonia. *Trees Struct Funct* 33:557–575. <https://doi.org/10.1007/s00468-018-1801-1>
- Garreaud RD, Vuille M, Compagnucci R, Marengo J (2009) Present-day South American climate. *Palaeogeogr Palaeoclimatol Palaeoecol*. <https://doi.org/10.1016/j.palaeo.2007.10.032>
- Garreaud R, Lopez P, Minvielle M, Rojas M (2013) Large-scale control on the Patagonian climate. *J Clim* 26:215–230. <https://doi.org/10.1175/JCLI-D-12-00001.1>
- Geladi P, Kowalski BR (1986) Partial least-squares regression: a tutorial. *Anal Chim Acta*. [https://doi.org/10.1016/0003-2670\(86\)80028-9](https://doi.org/10.1016/0003-2670(86)80028-9)
- Grissino-Mayer H (2001) Evaluating crossdating accuracy: a manual and tutorial for the computer program COFECHA. *Tree-ring Res*.
- Harris I, Osborn TJ, Jones P, Lister D (2020) Version 4 of the CRU TS monthly high-resolution gridded multivariate climate dataset. *Sci Data*. <https://doi.org/10.1038/s41597-020-0453-3>
- Holmes RL (1983) Program COFECHA user's manual. Laboratory of Tree-Ring Research. The University of Arizona, Tucson
- Jacques-Coper M, Brönnimann S (2014) Summer temperature in the eastern part of southern South America: its variability in the twentieth century and a teleconnection with Oceania. *Clim Dyn*. <https://doi.org/10.1007/s00382-013-2038-8>
- Jacques-Coper M, Garreaud RD (2015) Characterization of the 1970s climate shift in South America. *Int J Climatol*. <https://doi.org/10.1002/joc.4120>
- Jacques-Coper M, Brönnimann S, Martius O et al (2016) Summer heat waves in southeastern Patagonia: an analysis of the intraseasonal timescale. *Int J Climatol*. <https://doi.org/10.1002/joc.4430>
- Kalela-Brundin M (1999) Climatic information from tree-rings of *Pinus sylvestris* L. and a reconstruction of summer temperatures back to AD 1500 in Femundsmarka, eastern Norway, using partial least squares regression (PLS) analysis. *Holocene* 9:59–77. <https://doi.org/10.1191/095968399678118795>
- Llancabure JJ (2011) Relaciones entre el crecimiento de *Nothofagus betuloides* y el clima local y de gran escala en bosques subantárticos de la Isla Navarino. Tesis Ingeniero Forestal. Valdivia, Chile. Facultad de Ciencias Forestales y Recursos Naturales, Universidad Austral de Chile. 29 p.
- Marengo JA, Jones R, Alves LM, Valverde MC (2009) Future change of temperature and precipitation extremes in South America as derived from the PRECIS regional climate modeling system. *Int J Climatol*. <https://doi.org/10.1002/joc.1863>
- Marshall GJ (2003) Trends in the southern annular mode from observations and reanalyses. *J Clim*. [https://doi.org/10.1175/1520-0442\(2003\)016<4134:TITSAM>2.0.CO;2](https://doi.org/10.1175/1520-0442(2003)016<4134:TITSAM>2.0.CO;2)
- Marshall GJ, Orr A, van Lipzig NPM, King JC (2006) The impact of a changing Southern Hemisphere Annular Mode on Antarctic Peninsula summer temperatures. *J Clim*. <https://doi.org/10.1175/JCLI3844.1>
- Massaccesi G, Roig FA, Martínez Pastur GJ, Barrera MD (2008) Growth patterns of *Nothofagus pumilio* trees along altitudinal gradients in Tierra del Fuego, Argentina. *Trees Struct Funct*. <https://doi.org/10.1007/s00468-007-0181-8>
- Matskovsky V, Roig FA, Pastur GM (2019) Removal of a non-climatically induced seven-year cycle from *Nothofagus pumilio* tree-ring width chronologies from Tierra del Fuego, Argentina for their use in climate reconstructions. *Dendrochronologia* 57:125610. <https://doi.org/10.1016/j.dendro.2019.125610>
- McCarroll D, Young GH, Loader NJ (2015) Measuring the skill of variance-scaled climate reconstructions and a test for the capture of extremes. *Holocene* 25(4):618–626
- Meko D (1997) Dendroclimatic reconstruction with time varying predictor subsets of tree indices. *J Clim*. [https://doi.org/10.1175/1520-0442\(1997\)010<0687:DRWTVP>2.0.CO;2](https://doi.org/10.1175/1520-0442(1997)010<0687:DRWTVP>2.0.CO;2)
- Melvin TM, Briffa KR (2008) A "signal-free" approach to dendroclimatic standardisation. *Dendrochronologia* 26:71–86
- Morales MS, Cook ER, Barichivich J et al (2020) Six hundred years of South American tree rings reveal an increase in severe hydroclimatic events since mid-20th century. *Proc Natl Acad Sci*. <https://doi.org/10.1073/pnas.2002411117>
- Moy CM, Moreno PI, Dunbar RB, et al (2009) Climate change in southern South America during the last two millennia. In: Past climate variability in South America and surrounding regions. Springer, Dordrecht, 2009, pp 353–393.
- Mundo IA, Palazzini DA, Barotto AJ, Martínez-Pastur GJ, Barrera MD (2020) Dendroecology applied to silvicultural management in the southern patagonian forests: a case study from an experimental forest in Tierra del Fuego, Argentina. In: Pompa-García M, Camarero JJ (eds) Latin american dendroecology. Springer, Cham, pp. 317–330
- Neukom R, Luterbacher J, Villalba R et al (2011) Multiproxy summer and winter surface air temperature field reconstructions for southern South America covering the past centuries. *Clim Dyn* 37:35–51. <https://doi.org/10.1007/s00382-010-0793-3>
- Parnesan C (2006) Ecological and evolutionary responses to recent climate change. *Annu Rev Ecol Evol Syst* 37:637–669
- Paruelo JM, Jobbagy EG, Sala OE (1998) Biozones of Patagonia (Argentina). *Ecol Aust* 8(02):145–153
- Pedrerá A, Galindo-Zaldívar J, Ruiz-Constán A, Bohoyo F, Torres-Carbonell P, Ruano P, Maestro A, González-Castillo L (2014) The last major earthquakes along the Magallanes-Fagnano fault system recorded by disturbed trees (Tierra del Fuego, South America). *Terra Nova* 26(6):448–453
- Rabassa J, Heusser C, Rutter N (1989) Late-glacial and Holocene of argentine tierra del fuego. *Quat South Am Antarct Peninsula* 7:327–351

- Rayner NA, Parker DE, Horton EB et al (2003) Global analyses of sea surface temperature, sea ice, and night marine air temperature since the late nineteenth century. *J Geophys Res Atmos*. <https://doi.org/10.1029/2002jd002670>
- Reichstein M, Camps-Valls G, Stevens B et al (2019) Deep learning and process understanding for data-driven Earth system science. *Nature*. <https://doi.org/10.1038/s41586-019-0912-1>
- Roig FA, Villalba R (2008) Understanding climate from Patagonian tree rings. In: Rabassa J (ed) *Late Cenozoic of patagonia and tierra del fuego*. *Developments in Quaternary Sciences* 11, pp 411–435.
- Roig F, Roig C, Rabassa J, Boninsegna J (1996) Fuegian floating tree-ring chronology from subfossil *Nothofagus* wood. *Holocene* 6:469–476. <https://doi.org/10.1177/095968369600600410>
- Roig FA, Palmer JG, Cook ER, Boswijk G, Stahle D, Villalba R, D'Arrigo RD (2010) Long tree-ring records from the southern hemisphere. In: Payette S, Filion L (eds) *La dendroecologie: principes, methodes et applications*. Les Presses de l'Université Laval, Québec, pp 647–682
- Slivinski LC, Compo GP, Whitaker JS et al (2019) Towards a more reliable historical reanalysis: improvements for version 3 of the Twentieth Century Reanalysis system. *Q J R Meteorol Soc*. <https://doi.org/10.1002/qj.3598>
- Soto-Rogel P, Aravena JC (2017) Potencial dendroclimático de *Nothofagus betuloides* en la Cordillera de Darwin, Tierra del Fuego. *Chile Bosque* (Valdivia). <https://doi.org/10.4067/s0717-92002017000100016>
- Timilsena J, Piechota T (2008) Regionalization and reconstruction of snow water equivalent in the upper Colorado River basin. *J Hydrol*. <https://doi.org/10.1016/j.jhydrol.2007.12.024>
- Trenberth KE, Stepaniak DP (2001) Indices of El Niño evolution. *J Clim*. [https://doi.org/10.1175/1520-0442\(2001\)014%3c1697:LIOENO%3e2.0.CO;2](https://doi.org/10.1175/1520-0442(2001)014%3c1697:LIOENO%3e2.0.CO;2)
- Villalba R, Lara A, Boninsegna JA et al (2003) Large-scale temperature changes across the southern Andes: 20th-century variations in the context of the past 400 years. *Clim Change* 59:177–232
- Visbeck M (2009) A station-based southern annular mode index from 1884 to 2005. *J Clim*. <https://doi.org/10.1175/2008JCLI2260.1>
- Wigley TML, Briffa KR, Jones PD (1984) On the average value of correlated time series with applications in dendroclimatology and hydrometeorology. *J Clim Appl Meteorol*.

Publisher's Note Springer Nature remains neutral with regard to jurisdictional claims in published maps and institutional affiliations.